Engineering Structures 224 (2020) 111007

Contents lists available at ScienceDirect

Engineering Structures

journal homepage: www.elsevier.com/locate/engstruct

Modified frequency and spatial domain decomposition method based on maximum likelihood estimation

Çağlayan Hızal

Department of Civil Engineering, Izmir Institute of Technology, Izmir, Turkey

ARTICLE INFO

Keywords:
Operational modal analysis
Modal identification
Measurement noise
Modelling error
Mode shape estimation
Frequency domain decomposition
Maximum likelihood estimation

ABSTRACT

In this study, a Modified Frequency and Spatial Domain Decomposition (MFSDD) technique is developed for modal parameter identification, using output-only response measurements. According to the presented procedure, the most probable power spectral density matrix of the measured response (output PSD) is updated by a maximum likelihood estimation based on the observed data. Different from the available Frequency Domain Decomposition (FDD) techniques, a prediction error term which is associated with the measurement noise and modelling errors is included in the proposed methodology. In this context, a detailed discussion is provided from various aspects for the effect of measurement noise and modelling errors on the parameter estimation quality. Two numerical and two experimental analysis are conducted in order to demonstrate the effectiveness and accuracy of the proposed methodology under some extreme effects. The obtained results indicate that the proposed method shows very good performance in modal parameter estimation in case of noisy measurements.

1. Introduction

Over the past few decades, various modal identification approaches have been developed in the context of vibration based Structural Health Monitoring (SHM). Among these, Operational Modal Analysis (OMA) methods, which do not refer any information about the source of input motion (or excitation), are extensively implemented in SHM community. Various OMA techniques based on the physical, statistical or probabilistic interpretation of the measured response have been previously presented to literature. From this aspect, the available OMA applications can be basically classified as time and frequency domain methods.

As one of the most conventional time domain approaches, Natural Excitation Technique and Eigen System Realization Algorithm (NExT-ERA) proposes a two-stage solution which is composed by the combination of two-different techniques. Initially, the measured vibration data is processed and transformed by NExT to an equivalent free vibration response data. At the next step, the modal properties are extracted by ERA which constructs a linear state-space dynamical model based on the modal characteristics of the measured system [1].

Another time domain technique, Stochastic Subspace Identification (SSI), presents a statistical framework based on the sate-space representation of a linear dynamic model excited by a Gaussian White Noise signal. In the implementation of SSI, first, the state of the system is predicted by a Kalman filter application based on the outputs of the Hankel matrix, which is a special form of the collected response data (SSI-Data) or its covariance (SSI-Cov). After updating the system matrices by a linear regression of Kalman state sequences, the prediction errors are recovered [2,3]. Even though SSI appears as a more effective technique in comparison to NExT-Era, one can pertain some important difficulties in the implementation based on the model class selection, and/or extraction of possible modes.

A more sophisticated time-domain method, Bayesian Time Domain Approach (BTDA), proposes an alternative procedure making a probabilistic interpretation for the measured response. Essentially, BTDA assumes that the measured response follows a zero mean Gaussian distribution provided that the adequately long measurement duration. Thus, the modal parameters can be inferred by the maximization of a conditional probability density function (PDF) based on the observed time domain response [4]. In case of noisy measurements, BTDA can provide rather reliable results compared to SSI methods. Despite its effectiveness, however, BTDA may induce some serious problems in terms of the computational effort due to the difficulties in the construction of PDF in the time domain.

In comparison to time domain techniques, frequency domain methods are computationally less expensive since they mainly focus on narrow frequency bands in which the measured response is dominated by a few number of modes. Various frequency domain OMA methods are available in the literature, such as frequency domain maximum likelihood estimation [5,6], Power Spectral Density Transmissibility

E-mail address: caglayanhizal@iyte.edu.tr.

https://doi.org/10.1016/j.engstruct.2020.111007
Received 15 January 2020; Received in revised form 21 June 2020; Accepted 23 June 2020
Available online 04 September 2020

(PSDT) [7–9], and Bayesian Operation Modal Analysis (BAYOMA) [10,11].

Among the aforementioned frequency domain techniques, BAYOMA, which updates the modal parameters from a probabilistic model based on the observed data, comes forward as one of the most efficient algorithms. The most important advantage of BAYOMA is having capability to determine not only the most probable modal parameters but also to provide an uncertainty information for the identified values. Therefore, it has been incorporated by various SHM issues such as multi-setup measurements [12–14] and finite element model updating [15,16]. Despite its effectiveness, BAYOMA methods may also increase the computational time and effort since it needs the maximization of a multi-variate and highly nonlinear PDF. In addition to this, BAYOMA requires a posterior uncertainty quantification process, which make it an extremely challenging procedure for complex problems (i.e. closely spaced modes, multiple setup measurements).

Frequency Domain Decomposition (FDD) which is another widely known identification technique, appears as a good preference for OMA applications since it requires less computational effort compared to BAYOMA. In the classical implementation of FDD, modal frequencies are detected from the singular value (SV) or power spectral density (PSD) spectrum of the measured data by peak-picking, and the mode shape vector is updated as the singular vector of the output PSD matrix [17–19]. Therefore, FDD is not able to provide any information for the modal damping ratio in its classical form. To overcome this problem, a modified version, Enhanced Frequency Domain Decomposition (EFDD), has been presented by Brincker et al [20]. In EFDD, an equivalent time-domain response for a single mode is derived in a narrow band using the inverse Fast Fourier Transform (iFFT) of the frequency domain data. The resulting truncated time-domain data is considered as an approximated free vibration response for the corresponding mode, and then, the modal damping ratio is updated from the decay of motion of the generated truncated response. However, this modal damping estimation may cause biased errors during the generation of approximated time-domain response [21].

To improve the estimation quality of modal damping ratio, a Frequency and Spatial Domain Decomposition (FSDD) method has been presented to literature [21–23]. FSDD estimates the modal frequencies and damping ratios by minimizing a least squares equation based on the residual between the singular values of analytical and data driven output PSD matrices. The mode shapes, however, are determined by following the same procedure with classical FDD methods.

The effectiveness of FDD methods can also be adversely affected when some fundamental modelling assumptions such as stationary input data and small modal damping ratio are violated due to the heavy or non-classical damping and the source of excitations (e.g. earthquake effects). A novel approach, refined Frequency Domain Decomposition (rFDD) technique, has been presented by Pioldi et al. [24] to mitigate the errors in the damping estimation of the structures subjected to earthquake induced vibrations. The refinement of this methodology lies in some further post-processes on output PSD and correlation matrices, using Wiener-Khinchin approach or Welch's modified periodogram. In this context, an iterative procedure is employed to make more reliable parameter estimations [25]. Various modifications and extended implementations of rFDD technique are available in the literature [26–30].

Classical FDD methods are not able to quantify the identification errors deduced by some widely seen effects such as measurement noise and modelling errors, and this may also lead to less reliable estimations in case of extremely noisy measurements. To address this problem, a Modified Frequency and Spatial Domain Decomposition (MFSDD) method is presented in this study. Different from the available FDD approaches, the presented method works based on the reconfiguration of analytical output PSD matrix, using a probabilistic framework similar to Bayesian methods. As an important novelty, the method provides a prediction error induced by the noise effects due to the measurement process and modelling assumptions. Thus, the proposed method remarkably improves the modal parameter estimation quality compared to the available FSDD technique.

According to the proposed methodology, the analytical output PSD matrix is separated to uncoupled matrices by applying a singular value decomposition so that each one represents an equivalent single mode response within a selected narrow frequency band. Then, a PDF is defined in which the analytical output PSD matrix is considered as a mathematical expectation. Here, the mathematical expectation of output PSD is defined as a function of modal parameters (natural frequency, modal damping ratio and mode shape vector) and prediction error. Finally, the most probable modal parameters as well as the prediction errors are determined by a maximum likelihood estimation.

Two numerical and two experimental analysis are conducted to verify the effectiveness of the proposed method. In numerical examples, a detailed investigation is presented to find out the source of prediction (or identification) errors due to the effects of measurement noise, earthquake input and heavy damping. Then, the presented method is implemented on two different benchmark studies for experimental verification. According to the obtained results, it is observed that the proposed method shows better performance in comparison with available FSDD technique, under large noise effects.

2. Theoretical background of frequency and spatial domain decomposition method

The frequency domain equation of motion of a linear multi-degree of freedom (MDOF) system subjected to ambient nodal forces and/or base excitations can be written as below.

$$\mathbf{M}\ddot{\mathbf{Y}}(\omega_k) + \mathbf{C}\dot{\mathbf{Y}}(\omega_k) + \mathbf{K}\mathbf{Y}(\omega_k) = \mathbf{F}(\omega_k) \tag{1}$$

where $\mathbf{Y}(\omega_k)$, $\dot{\mathbf{Y}}(\omega_k)$, $\ddot{\mathbf{Y}}(\omega_k)$ represent the $N_d \times 1$ sized displacement, velocity and acceleration response vectors (outputs), $\mathbf{F}(\omega_k) = N_d \times 1$ sized frequency domain force vector (input), and $\mathbf{M}$, $\mathbf{C}$ and $\mathbf{K}$ denote the $N_d \times N_d$ sized mass, damping and stiffness matrix of the considered MDOF system, respectively. In addition, N_d = number of degrees of freedom (DOF), k = step number for a discrete frequency, and ω_k = discrete excitation frequency at step k. Here, the relation between the unknown inputs (or references), and the PSD of the measured response can be defined by [20]:

$$\mathbf{G}_{yy}(\omega_k) = \overline{\mathbf{H}}(\omega_k)\mathbf{G}_{xx}(\omega)\mathbf{H}^T(\omega_k) \tag{2}$$

where $\mathbf{G}_{yy}(\omega_k) = N \times N$ sized output PSD matrix, $\mathbf{G}_{xx}(\omega_k) = N \times N$ sized input PSD matrix, and N = number of measured DOF (here, all output measurements are considered as reference). In addition, $\mathbf{H}(\omega_k)$ represents the $N \times N$ sized Frequency Response Function (FRF) which can be written in the pole-residue form as follows [20].

$$\mathbf{H}(\omega_k) = \sum_{n=1}^{N_d} \frac{\mathbf{R}_n}{\mathbf{i}\omega_k - \lambda_n} + \frac{\bar{\mathbf{R}}_n}{\mathbf{i}\omega_k - \bar{\lambda}_n} \tag{3}$$

in which $\lambda_n = \sigma_n + \mathbf{i}\omega_{dn}$, and $\mathbf{R}_n = \varphi_n \Gamma_n$ denote the n^{th} pole and residue, and $\bar{\lambda}_n$, $\bar{\mathbf{R}}_n$ indicate the conjugates. In addition, φ_n, σ_n, ω_{dn} and Γ_n represents the modal shape vector, damping factor, damped modal frequency and modal participation vector for the n^{th} mode, respectively.

$$\begin{aligned} &\sigma_n = \xi_n \omega_n; \\ &\omega_{dn} = \omega_n \sqrt{1 - \xi_n^2}; \\ &\Gamma_n = \frac{\varphi_n^*}{\varphi_n^* \mathbf{M} \varphi_n} \end{aligned} \tag{4}$$

where ω_n and ξ_n represent the n^{th} modal angular frequency and damping ratio, and the superscript "*" denotes the conjugate and transpose. Thus, the output PSD can be analytically defined by [20]:

$$\mathbf{G}_{yy}(\omega_k) = \sum_{m=1}^{N_d}\sum_{n=1}^{N_d}\left[\frac{\mathbf{R}_m}{\mathbf{i}\omega_k - \lambda_m} + \frac{\bar{\mathbf{R}}_m}{\mathbf{i}\omega_k - \lambda_m^*}\right]\mathbf{G}_{xx}(\omega)\left[\frac{\bar{\mathbf{R}}_n}{\mathbf{i}\omega_k - \lambda_n} + \frac{\mathbf{R}_n^*}{\mathbf{i}\omega_k - \lambda_n^*}\right] \tag{5}$$

where, $\lambda_n^* = \bar{\lambda}_n$. For a stationary Gaussian process, the excitation vector can be represented by independent and identically distributed (*i.i.d.*) random variables. It can be deduced from the here that the resulting output PSD becomes a positive definite block diagonal matrix whose elements correspond to a constant scalar, G_{xx}. Applying the Heaviside's partial fraction expansion for the right hand-side of Eq. (5), the output PSD matrix can be arranged as below [24].

$$\mathbf{G}_{yy}(\omega_k) = \sum_{n=1}^{N_d}\left[\frac{\mathbf{A}_n}{\mathbf{i}\omega_k - \lambda_n} + \frac{\mathbf{A}_n^*}{-\mathbf{i}\omega_k - \lambda_n^*} + \frac{\bar{\mathbf{A}}_n}{\mathbf{i}\omega_k - \lambda_n^*} + \frac{\mathbf{A}_n^T}{-\mathbf{i}\omega_k - \lambda_n}\right] \tag{6}$$

where $\mathbf{A}_n$ denotes a Hermitian matrix, which can be defined by the following equation.

$$\mathbf{A}_n = \sum_{m=1}^{N_d}\left[\frac{\mathbf{R}_m}{-\lambda_n - \lambda_m} + \frac{\bar{\mathbf{R}}_m}{-\lambda_n - \lambda_m^*}\right]G_{xx}\mathbf{R}_n^T \tag{7}$$

For lower damping levels (e.g. about 1–2%), Eq. (7) can be approximated by the following expression, in the vicinity of n^{th} mode, assuming $\lambda_n = -\xi_n\omega_n + \mathbf{i}\omega_{dn} \cong -\xi_n\omega_n + \mathbf{i}\omega_n$, [24].

$$\mathbf{A}_n \cong \frac{\Gamma_n G_{xx}\Gamma_n^*}{2\sigma_n}\varphi_n\varphi_n^* \tag{8}$$

Substituting Eq. (8) into (6), and after some arrangements, the analytical value of output PSD can be defined by the following equation, within a narrow frequency band [21].

$$\mathbf{G}_{yy}(\omega_k) \cong \sum_{n=1}^{N_m}\varphi_n\,\mathrm{Re}\left(\frac{2c_n}{\mathbf{i}\omega_k - \lambda_n}\right)\varphi_n^* \tag{9}$$

where $c_n = \Gamma_n G_{xx}\Gamma_n^*/2\sigma_n$, and N_m = number of possible modes within the selected narrow band (in case of single mode, $N_m = 1$). Here, the singular value decomposition of the output PSD is given by:

$$\mathbf{G}_{yy}(\omega_k) = \mathbf{U}(\omega_k)\mathbf{S}(\omega_k)\mathbf{U}^*(\omega_k) \tag{10}$$

where $\mathbf{U} = [\mathbf{u}_1, \cdots, \mathbf{u}_N]$ represents an $N \times N$ sized unitary matrix spanning the singular vectors, and $\mathbf{S}$ is an $N \times N$ sized diagonal matrix that contains the real singular values. In the vicinity of n^{th} modal frequency, an equivalent single mode response can be achieved by [21].

$$\begin{aligned}&\mathbf{G}_{yy}(\omega_k) \underset{\omega_k \to \omega_n}{\cong} \mathbf{u}_n(\omega_n)s_{nn}(\omega_k)\mathbf{u}_n^*(\omega_n);\\ &s_{nn}(\omega_k) = \mathrm{Re}\left(\tfrac{2c_n}{\mathbf{i}\omega_k - \lambda_n}\right);\\ &\mathbf{u}_n(\omega_n) = \varphi_n\end{aligned} \tag{11}$$

Here, the singular values should be sorted in the descending order. Thus, the mode shape vector is calculated as a singular vector of $\mathbf{G}_{yy}(\omega_k)$. At the next step, a filtered output that corresponds to an equivalent single degree of freedom (SDOF) response for the n^{th} mode can be represented by $\varphi_n^*\mathbf{G}_{yy}(\omega_k)\varphi_n$. Here, a residual can be defined based on the discrepancy between the filtered response and its analytical value, $\mathrm{Re}(2c_n/(\mathbf{i}\omega_k - \lambda_n))$. Thus, the optimal natural frequencies and damping ratios can be calculated by minimizing the following objective function.

$$\arg\min_{\omega_n,\xi_n}\left\{\left[\varphi_n^*\mathbf{G}_{yy}(\omega_k)\varphi_n - \mathrm{Re}\left(\frac{2c_n}{\mathbf{i}\omega_k - \lambda_n}\right)\right]^2\right\} \tag{12}$$

In comparison to EFDD, FSDD shows better performance in terms of the estimation quality of modal frequencies and damping ratios, especially in case of closely spaced modes. The mode shape estimation, however, follows the same procedure with classical FDD methods. In case of large noise effects, the quality of estimated mode shapes might be adversely affected due to the decrease in the frequency resolution in SV or PSD spectrum. In addition, some extreme effects such as heavy damping and earthquake induced excitations may also increase the modelling errors, leading to noisy data. Therefore, a modified methodology that addresses the possible solutions for such kind of problems is developed here, in order to improve the effectiveness of FSDD.

3. Proposed modified frequency and spatial domain decomposition method

In this section, the theoretical framework of the proposed modified technique is introduced. Although the proposed method is motivated from FSDD, it is based on a quite different computational strategy. According to this strategy, the analytical output PSD is considered as *statistically expected* value within a resonant frequency band selected for the possible mode(s). The method assumes small damping ratios and orthogonal mode shapes, and it is capable of identifying the closely spaced modes. For this purpose, the output PSD is separated to uncoupled matrices so that each one represents an equivalent single mode response within the selected frequency band. At this stage, the uncoupled matrices can be obtained by taking the singular value decomposition of the output PSD, $\mathbf{G}_{yy}(\omega_k)$, as below.

$$\begin{aligned}&\mathbf{G}_{yy}(\omega_k) \cong \textstyle\sum_{n=1}^{N_m}\mathbf{G}_{yy}^{(n)}(\omega_k)\\ &\mathbf{G}_{yy}^{(n)}(\omega_k) = \mathbf{u}_n(\omega_k)s_{nn}(\omega_k)\mathbf{u}_n^*(\omega_k)\end{aligned} \tag{13}$$

where $\mathbf{G}_{yy}^{(n)}(\omega_k)$ = uncoupled output-PSD that represents the n^{th} modal response only. In the vicinity of n^{th} modal frequency, a statistically expected value for $\mathbf{G}_{yy}^{(n)}(\omega_k)$ can be defined by:

$$E\left[\mathbf{G}_{yy}^{(n)}(\omega_k)\right] \underset{\omega_k \to \omega_n}{=} \varphi_n\bar{c}_n\alpha_n(\omega_k, \omega_n, \xi_n)\varphi_n^* + \delta_n\mathbf{I}_N \tag{14}$$

where "$\bar{c}_n = \Gamma_n G_{xx}\Gamma_n^*$" and "$\alpha_n(\omega_k, \omega_n, \xi_n) = \mathrm{Re}([\sigma_n(\mathbf{i}\omega_k - \lambda_n)]^{-1})$." $\mathbf{I}_N = N \times N$ sized identity matrix, and $E[.]$ = mathematical expectation operator. In addition, δ_n represents a modelling error caused by the violation of fundamental modelling assumptions such as small damping ratio, stationary input data and orthogonality of mode shapes. Assuming that the defined uncoupled PSD matrices are statistically independent, the expected value of $\mathbf{G}_{yy}(\omega_k)$ can be obtained by,

$$E\left[\mathbf{G}_{yy}(\omega_k)\right] = \sum_{n=1}^{N_m}E\left[\mathbf{G}_{yy}^{(n)}(\omega_k)\right] + \varepsilon_m\mathbf{I}_N \tag{15}$$

where ε_m indicates the *measurement noise* (channel noise) due to the instrumentation and/or data acquisition process. Here, the measurement noise and modelling error terms can be modeled as diagonal matrices by considering them as *i.i.d.* random variables [11]. Thus, $E\left[\mathbf{G}_{yy}(\omega_k)\right]$ can be written as below by using Eqs. (14) and (15).

$$E\left[\mathbf{G}_{yy}(\omega_k)\right] = \sum_{n=1}^{N_m}\bar{c}_n\alpha_n(\omega_k, \omega_n, \xi_n)\varphi_n\varphi_n^* + \Delta_e\mathbf{I}_N \tag{16}$$

where Δ_e represents the *prediction error* in the estimation of $E\left[\mathbf{G}_{yy}(\omega_k)\right]$. Here, the prediction error term can also be modeled as a diagonal matrix by the combination of modelling errors and measurement noise ($\Delta_e = \varepsilon_m + \sum_{n=1}^{N_m}\delta_n$).

Under the ambient vibration effects, it can be assumed that the Fast Fourier Transform (FFT) of measured data follows a zero mean Gaussian distribution. Thus, the resulting output PSD follows a complex central Wishart distribution conditional to the modal parameters and prediction error, which is given by [31]:

$$p(\mathbf{G}_{yy}(\omega_k)|\ \theta, \Delta_e) = \prod_k\frac{\pi^{-\frac{N(N-1)}{2}}}{|E\left[\mathbf{G}_{yy}(\omega_k)\right]|}\exp\{-tr(E\left[\mathbf{G}_{yy}(\omega_k)\right]^{-1}\mathbf{G}_{yy}(\omega_k))\} \tag{17}$$

where $\theta = [\{\omega_1, \xi_1, \bar{c}_1, \varphi_1^*\}, \ldots, \{\omega_{N_m}, \xi_{N_m}, \bar{c}_{N_m}, \varphi_{N_m}^*\}]$ represents the set of

modal parameters to be estimated by the maximization of Eq. (17). Due to convenience, the maximum likelihood estimator given in Eq. (17) can be rewritten in terms of the negative-logarithm likelihood function as follows:

$$L(\theta, \Delta_e) = -ln[p(\mathbf{G}_{yy}(\omega_k)|\ \theta, \Delta_e)] = \frac{N_\omega N(N-1)}{2} ln\pi + \sum_k ln\ |E[\mathbf{G}_{yy}(\omega_k)]| + \sum_k tr(E[\mathbf{G}_{yy}(\omega_k)]^{-1}\mathbf{G}_{yy}(\omega_k)) \tag{18}$$

where N_ω = number of discrete excitation frequencies (number of data) within the selected frequency band. Thus, the most probable value (MPV) of θ can be achieved by minimizing Eq. (18). In this minimization process, however, an equality constraint is required for the mode shape vector in order to keep valid the unitary matrix assumption during the singular value decomposition. By inclusion of this equality constraint, an objective function can be derived for θ and Δ_e, as below.

$$J(\theta, \Delta_e, \beta) = \sum_k \ln\ |E[\mathbf{G}_{yy}(\omega_k)]| + \sum_k tr(E[\mathbf{G}_{yy}(\omega_k)]^{-1}\mathbf{G}_{yy}(\omega_k)) + \sum_{n=1}^{N_m} \beta_n(1-\varphi_n^*\varphi_n) \tag{19}$$

where $\beta = [\beta_1, ...,\beta_{N_m}]$ denote the set of Lagrange multipliers that enforce the unit Euclidian norm for the mode shape vectors.

The objective function given in Eq. (19) requires the calculation of inverse and determinant terms of $\mathbf{G}_{yy}(\omega_k)$ recursively, resulting in a considerable increase in the computational effort during the minimization process [32]. Instead, these terms can be directly calculated in a pre-process using the matrix inversion and determinant lemma, as shown below [32,33].

$$E[\mathbf{G}_{yy}(\omega_k)]^{-1} = \sum_{n=1}^{N_m} \bar{c}_n^{-1}\alpha_n^{-1}(\omega_k, \omega_n, \xi_n)\varphi_n\varphi_n^* + \Delta_e^{-1}(\mathbf{I}_N - \sum_{n=1}^{N_m}\varphi_n\varphi_n^*)$$
$$|E[\mathbf{G}_{yy}(\omega_k)]| = \sum_{n=1}^{N_m}[\bar{c}_n\alpha_n(\omega_k, \omega_n, \xi_n)]\Delta_e^{(N-N_m)} \tag{20}$$

Substituting Eq. (20) into Eq. (19), and after some arrangements yields:

$$J(\theta,\ \Delta_e,\ \beta) = \sum_{n=1}^{N_m}\sum_k \ln\bar{\alpha}_n(\omega_k, \omega_n, \xi_n) + \{N_\omega(N-N_m)\ln\Delta_e + \Delta_e^{-1}\sum_k tr(\mathbf{G}_{yy}(\omega_k)[\mathbf{I}_N - \sum_{n=1}^{N_m}\varphi_n\varphi_n^*])\} + \sum_{n=1}^{N_m}\{N_\omega\ln\bar{c}_n + \sum_k \bar{c}_n^{-1}\bar{\alpha}_n(\omega_k, \omega_n, \xi_n)^{-1}\varphi_n^*\mathbf{G}_{yy}(\omega_k)\varphi_n\} + \sum_{n=1}^{N_m}\beta_n(1-\varphi_n^*\varphi_n) \tag{21}$$

It is possible to obtain the MPV of $\{\bar{c}_n, \varphi_n^*, \Delta_e\}$ in a closed-form by a gradient based minimization of the objective function defined in Eq. (21). However, a similar closed-form solution for $\{\omega_n,\xi_n\}$ cannot be obtained by direct differentiation of the objective function [10]. Therefore, it might be more convenient to update $\{\omega_n,\xi_n\}$ after evaluating the MPV of $\{\bar{c}_n, \varphi_n^*, \Delta_e\}$.

Taking the first order gradient of Eq. (21) with respect to Δ_e, the most probable prediction error can be obtained by the following equation.

$$\nabla_{\Delta_e}J(\theta,\ \Delta_e,\ \beta) = N_\omega(N-N_m)\Delta_e^{-1} + \Delta_e^{-2}\sum_k tr(\mathbf{G}_{yy}(\omega_k)[\mathbf{I}_N - \sum_{n=1}^{N_m}\varphi_n\varphi_n^*]) = 0$$
$$\Rightarrow \hat{\Delta}_e = \frac{\sum_k tr(\mathbf{G}_{yy}(\omega_k)[\mathbf{I}_N - \sum_{n=1}^{N_m}\varphi_n\varphi_n^*])}{N_\omega(N-N_m)} \tag{22}$$

where "^" represents the MPV. Similarly, minimization of Eq. (21) with respect to $\bar{c}_n$ gives

$$\nabla_{\bar{c}_n}J(\theta, \Delta_e, \beta) = N_\omega\bar{c}_n^{-1} - \bar{c}_n^{-2}\sum_k \bar{\alpha}(\omega_k, \omega_n, \xi_n)^{-1}\varphi_n^*\mathbf{G}_{yy}(\omega_k)\varphi_n = 0$$
$$\Rightarrow \hat{\bar{c}}_n = N_\omega^{-1}\sum_k \bar{\alpha}(\omega_k, \omega_n, \xi_n)^{-1}\hat{\varphi}_n^*\mathbf{G}_{yy}(\omega_k)\hat{\varphi}_n \tag{23}$$

To obtain the MPV of mode shape vector, the objective function can be arranged as below.

$$J(\theta_n, \beta_n) = \hat{\Delta}_e^{-1}\sum_k \varphi_n^*\mathbf{G}_{yy}(\omega_k)\varphi_n\left(1 + \frac{\hat{\Delta}_e}{\bar{c}_n\bar{\alpha}(\omega_k, \omega_n, \xi_n)}\right) + \beta_n(1-\varphi_n^*\varphi_n) + C_1 \tag{24}$$

where C_1 indicates the constant terms, which do not depend on φ_n. Near the resonant frequency for the n^{th} mode ($\omega_k \to \omega_n$), it can be assumed that $\hat{\Delta}_e/\bar{c}_n\bar{\alpha}(\omega_k, \omega_n, \xi_n) \ll 1$, [10]. By making use of this assumption and neglecting the constant terms, Eq. (24) can be arranged as below.

$$J(\varphi_n, \beta_n) = \hat{\Delta}_e^{-1}\sum_k \varphi_n^*\mathbf{G}_{yy}(\omega_k)\varphi_n + \beta_n(1-\varphi_n^*\varphi_n) \tag{25}$$

Taking the first order gradient of Eq. (25) with respect to φ_n gives:

$$\nabla_{\varphi_n}J(\varphi_n, \beta_n) = \sum_k \mathbf{G}_{yy}(\omega_k)\varphi_n - \bar{\beta}_n\varphi_n = 0 \tag{26}$$

Solving Eq. (26) for $\varphi_n = \hat{\varphi}_n$ results in the following eigenvalue equation.

$$\left[\sum_k \mathbf{G}_{yy}(\omega_k)\right]\hat{\varphi}_n = \bar{\beta}_n\hat{\varphi}_n \tag{27}$$

where $\bar{\beta}_n = \hat{\varphi}_n^*[\sum_k \mathbf{G}_{yy}(\omega_k)]\hat{\varphi}_n$. Here, it should be stated that the singular vectors and eigenvectors of $\sum_k \mathbf{G}_{yy}(\omega_k)$ are identical since the output PSD matrices are positive definite Hermitian. Thus, the most probable mode shape vectors can be directly updated as the singular vectors (equivalent of eigenvector) of cumulative output PSD matrices, $\sum_k \mathbf{G}_{yy}(\omega_k)$. In case of closely spaced modes ($N_m > 1$), the singular vectors that correspond to the largest N_m singular values can be updated as most probable mode shapes.

After obtaining the MPV of $\{\bar{c}_n, \varphi_n^*, \Delta_e\}$, a condensed objective function for the n^{th} modal frequency and damping ratio can be derived by the re-arrangement of Eq. (21). To this end, substituting $\{\hat{c}_n, \hat{\varphi}_n^*, \hat{\Delta}_e\}$ into Eq. (21) leads to:

$$J(\omega_n, \xi_n) = \sum_k \ln\bar{\alpha}(\omega_k, \omega_n, \xi_n) + N_\omega\ln[\sum_k \bar{\alpha}(\omega_k, \omega_n, \xi_n)^{-1}\hat{\varphi}_n^*\mathbf{G}_{yy}(\omega_k)\hat{\varphi}_n/N_\omega] + C_2 \tag{28}$$

where C_2 represents the constant terms, which are irrelevant to ω_n and ξ_n. Thus, $\hat{\omega}_n$ and $\hat{\xi}_n$ can be estimated by an unconstrained numerical optimization of Eq. (28).

4. Summary of procedure

This study presents an output only identification procedure, based on the maximum likelihood estimation of modal parameters within narrow-frequency bands selected for the possible vibration modes. Therefore, as a first step, the possible modes and the corresponding bandwidths should be selected. For the frequency domain modal identification, an automated mode detection and bandwidth selection procedure is not available in the literature. Instead, a more intuitional approach can be implemented to determine the possible vibration modes and corresponding bandwidths [14].

Using the peak-picking method, the possible vibration modes can be detected on SV or PSD spectrum of the measured data. Here, different from the available FDD techniques, the modal parameters (especially the mode shape vector) estimated by MFSDD are not sensitive to the selected peaks. This procedure is only required to determine roughly the locations of possible modes. Selection of the bandwidths, however, may require a more sophisticated procedure.

Previous FDD applications implements a MAC based filtering process for bandwidth selection, spanning 90% proximity to the mode shape at the resonant frequency. However, this procedure requires a series of SV decompositions at the excitation frequencies neighbored to peak response. On the other hand, Au [32] proposes an optimal bandwidth selection in the range of 10–20% of the peak response frequency, based on the results obtained by BAYOMA.

In case of small damping ratio, a relatively narrow spectral bell

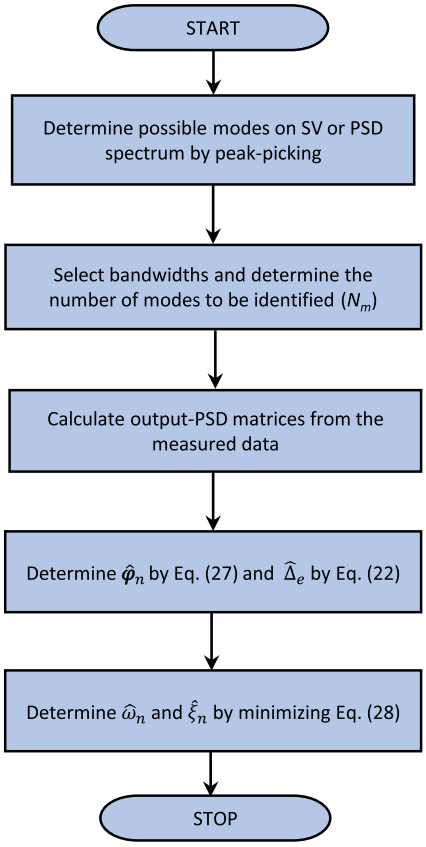

Fig. 1. Flowchart for the proposed MFSDD technique.

curve can be expected for the resonant frequency band. Therefore, a proper bandwidth should be selected for such a case so that it covers the bell curve in the SV spectrum. In case of larger damping ratio and/or noisy measurement data, however, a broader spectral bell curve may appear in the spectrum plot. In such a case, the proposition by Au [32] would be more reasonable. Considering both scenarios, this study suggests a bandwidth selection which covers the spectral bell curve and remains in the range of 10–20% of the peak response frequency.

The number of modes should be identified within the selected bandwidth can also be estimated from SV or PSD spectrum. If multiple peaks are visible within the selected bandwidth, the possibility of closely spaced modes should be brought to mind. In such a case, each identified uncoupled-PSD matrix will correspond to a single mode response equivalent to a closely spaced mode within the selected band. A flowchart for the overall procedure of the proposed MFSDD technique is presented in Fig. 1.

5. Numerical and experimental verification

In this section, two numerical and two field data examples are presented in order to find out the performance of the proposed method. In this context, the given numerical examples mainly concern the effect of pure measurement noise and modelling errors on the modal parameter estimation quality. Here, the first numerical example investigates the pure measurement noise effect on the quality of identified parameters. In the second numerical example, the modelling error effects due to the earthquake input, heavy damping, and closely spaced modes are investigated. Finally, two real data examples are presented for experimental verification of the proposed MFSDD technique.

5.1. Numerical analysis 1: Effect of measurement noise

A numerical model for a ten-story shear frame structure is generated with uniform inter-story stiffness of $k = 450\ kN/m$, and uniform mass of $m = 250\ kg$. The first five natural frequencies of the generated model are calculated as 1.009, 3.005, 4.934, 6.752 and 8.4201 Hz. This numerical application concerns the effect of pure measurement noise, in terms of the modal signal to noise ratio (*snr*), under the light damping and low amplitude ambient vibrations. Therefore, the modal damping ratio is considered as 1% for all modes. In addition, it is assumed that the considered model is subjected to *i.i.d.* Gaussian forces, resulting a $1\mu g^2/Hz$ of one-sided spectral density of modal excitation for all modes.

Acceleration response at each floor level is acquired with 250 *Hz* sampling frequency and 300 s duration. The acquired acceleration responses are then contaminated by *i.i.d.* Gaussian white noises generated with the one-sided spectral densities of 0.25, 0.5, 2.5, 5, 25, 50 and 250 $\mu g^2/Hz$, respectively. Thus, the resulting modal *snr* values are being set to 10000, 5000, 1000, 500, 100, 50 and 10, respectively. For comparison purposes, the modal parameters of the presented numerical model are identified by using MFSDD, FSDD, and SSI-Cov algorithms. Here, all identification procedures are performed by means of an in-house MATLAB [34] program coded for the considered techniques.

The SV spectra obtained from the simulated responses are presented in Fig. 2. As it was stated previously, the measurement noise is considered to appear during the data acquisition process. Such kind of noise effects may stem from the sensor (accelerometer) sensitivity, signal transmission cables or data acquisition device. Subsequently, these noise effects can be directly transmitted to collected analogue data [32]. Therefore, the measurement noise appears as one of the challenging parameters frequently confronted in OMA. From this perspective, it can be observed from the presented spectra that the larger measurement noise creates a significant decrease in the signal qualities and makes it more difficult to distinguish the spectral bell curves.

Table 1 and Table 2 present the relative deviations for identified modal frequencies and damping ratios, respectively. Here, the relative deviations are defined by:

$$\Delta f = \left(\frac{\hat{f}_n}{f_{n,act}} - 1\right) \times 100(\%)$$
$$\Delta \xi = \left(\frac{\hat{\xi}_n}{\xi_{n,act}} - 1\right) \times 100(\%) \tag{29}$$

where $f_{n,act}$ and $\xi_{n,act}$ denote the actual values of n^{th} natural frequency and modal damping ratio. At first view, it is seen that the identified modal frequencies show minor deviations at increasing noise levels. On the other hand, the damping ratios have a divergence up to 230% and 61% for FSDD and SSI-Cov, respectively. Deviations in MFSDD, however, remain considerably less (about 15%) in comparison to FSDD and

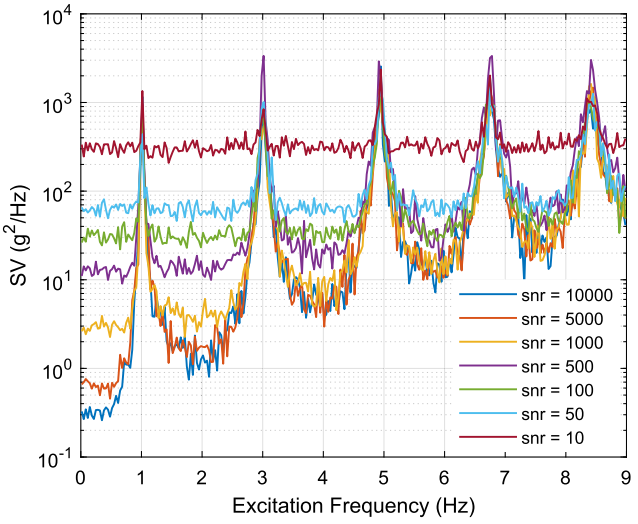

Fig. 2. SV spectrum for generated responses.

Table 1
Relative deviations for identified modal frequencies, Δf (%).

Mode Number	snr = 1000			snr = 100			snr = 10		
	MFSDD	FSDD	SSI-Cov	MFSDD	FSDD	SSI-Cov	MFSDD	FSDD	SSI-Cov
1	0.10	0.30	0.40	0.30	0.40	0.50	0.50	0.79	1.29
2	0.02	0.40	0.17	0.03	−0.13	−0.17	0.07	0.30	0.47
3	0.01	0.04	0.04	0.10	0.08	0.10	0.14	0.16	0.20
4	0.04	−0.03	−0.01	0.01	0.01	−0.03	−0.01	0.07	0.33
5	0.01	−0.01	0.03	0.04	−0.02	0.03	0.08	0.31	0.36

SSI-Cov. Thus, it can be clearly deduced that the proposed method shows better performance compared to FSDD and SSI-Cov, when the pure measurement noise effect is considered only.

Due to the fact that small damping ratios and white noise excitations are considered in this numerical example, minor modelling errors can be expected. Therefore, one can be concluded that the identified prediction errors highly reflect the pure measurement noise for this particular example. To illustrate this situation, variations in the identified prediction errors with respect to the actual measurement noise values are presented in Fig. 3. When the actual measurement noise values are smaller than 1 $\mu g^2/Hz$, modelling errors become more dominant compared to the prediction errors. For the larger noise values, however, the identified prediction errors perfectly match with the actual noise, as a result of the fact that the modelling errors are negligibly small compared to the measurement noise. From this aspect, it can be deduced that the presented method is capable of identifying the measurement noise with a high level of accuracy. On the other hand, the modelling errors may not be identified correctly even the source of these errors are well-defined in the analytical model. The estimation of modelling errors, therefore, become a more challenging problem in comparison to the measurement noise.

Fig. 4 presents the variations in the relative errors for identified modal shape vectors obtained by MFSDD, FSDD and SSI-Cov, respectively. Here, the relative errors for mode shapes are calculated by using the following equation.

$$e_r = |1 - MAC(\hat{\varphi}_n, \phi_n)| \times 100(\%) \tag{30}$$

where ϕ_n = analytical value of the n^{th} modal shape vector, and MAC(**x**, **y**) represents the modal assurance criterion between the vectors **x** and **y**. According to results, it is observed that the relative error in the mode shapes obtained by MFSDD are significantly small under large measurement noise effects (lower *snr* values). Here, the most dramatic difference is observed for the results obtained by FSDD. This difference can be considered to be stem from the noisy plots in the spectral-bell curve. Due to these plots, it might be more difficult to detect resonant frequencies on the SV spectrum. This situation is better illustrated in Fig. 5 which presents the variations in MAC values, between $\mathbf{u}(\omega_k)$ and the actual value of first modal shape vector.

Fig. 5 indicates that the calculated MAC values show a significant decrease and fluctuations around the resonant frequency, under large noise effects. These fluctuations make it more difficult to perceive the peak response for the optimal mode shape estimation. Therefore, a sensitive trial and error methodology and/or an extensive signal processing procedure becomes necessary to determine the optimal value. The proposed method, however, does not require such a sensitive peak-response selection procedure for the mode shapes. Instead, the optimal mode shapes are updated from the cumulative output PSD matrix with a better level of accuracy.

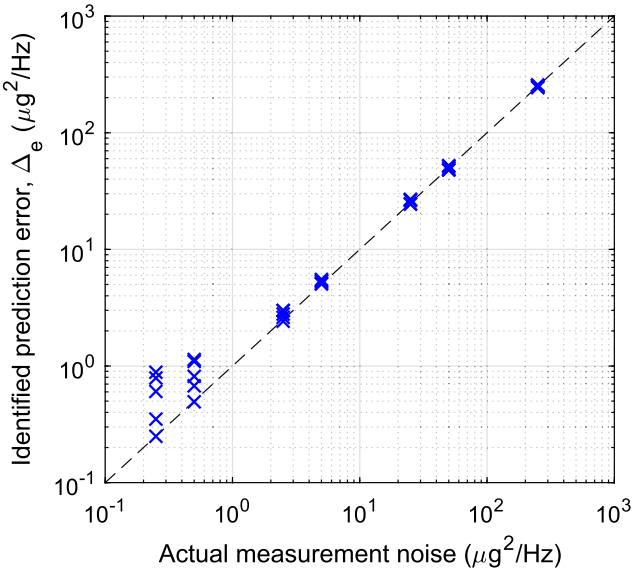

Fig. 3. Variations in the identified prediction error with respect to measurement noise.

5.2. Numerical analysis 2: Earthquake induced motion and heavy damping

A further investigation for the source of identification errors is presented in this section, using a numerical model of a reinforced concrete (RC) shear frame adapted from Villaverde and Koyama [35]. Fundamental properties of the model are summarized in Table 3. The considered example includes closely spaced modes and heavy modal damping ratios. Therefore, large amount of modelling errors can be expected, especially at the higher modes. In this context, this numerical model was previously investigated by Pioldi et al. [24] to validate their rFDD methodology, using a series of earthquake input motions

Table 2
Relative deviations for identified modal damping ratios, $\Delta\xi$ (%).

Mode Number	snr = 1000			snr = 100			snr = 10		
	MFSDD	FSDD	SSI-Cov	MFSDD	FSDD	SSI-Cov	MFSDD	FSDD	SSI-Cov
1	0.06	−8.21	2.08	2.16	29.11	18.63	6.88	117.40	−52.16
2	1.38	9.98	3.61	4.01	93.29	−27.09	10.53	230.31	−44.25
3	0.02	1.14	3.24	1.78	4.36	11.27	1.21	110.74	37.72
4	0.18	8.33	2.55	1.44	50.92	24.49	2.39	115.52	39.69
5	1.21	−15.27	7.49	7.25	49.53	19.82	16.48	185.33	61.64

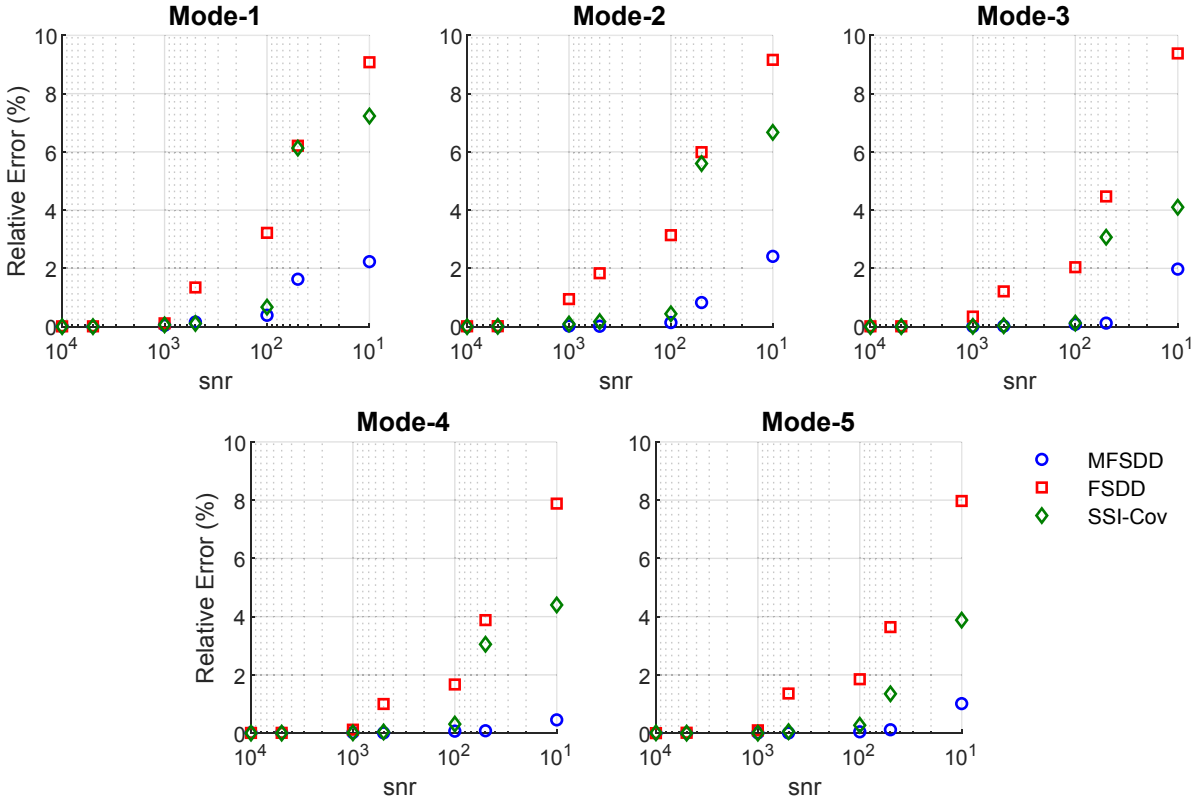

Fig. 4. Variations in the relative error for the identified modal shape vectors.

[27,28,30]. For comparison purposes, three different earthquakes, El Centro (1940), Northridge (1994) and Tabas (1978), which were previously utilized by Pioldi and Rizzi [28], are considered in this study.

Modal parameters of the considered RC structure are estimated by means of the proposed MFSDD technique considering the all modes of vibration. The identified modal parameters are then compared to the results reported by Pioldi and Rizzi [28]. Here, Pioldi and Rizzi [28] implemented two different algorithms, namely rFDD and SSI-Cov, making a comparison in terms of the convergence rate under the effects of earthquake motion and heavy modal damping. The effectiveness of rFDD method has been well-established in the literature. Therefore, the results by rFDD can be considered here as reference values for MFSDD.

Fig. 6 shows the absolute relative errors calculated for the identified natural frequencies and damping ratios as well as the MAC values between the identified mode shapes and their actual values. Here, the major difference in the absolute errors are observed in the results by

Table 3
Fundamental properties of the numerical model [28].

Story number	Stiffness (MN/m)	Mass (tons)	Mode number	$f_{n,act}(Hz)$	$\xi_{n,act}(\%)$
1	62.47	179	1	0.500	2.50
2	59.26	170	2	1.326	3.50
3	56.14	161	3	2.151	5.16
4	53.02	152	4	2.934	6.83
5	49.91	143	5	3.653	8.40
6	46.79	134	6	4.292	9.81
7	43.70	125	7	4.836	11.01
8	40.55	116	8	5.272	11.98
9	37.43	107	9	5.590	12.69
10	34.31	98	10	5.787	13.13

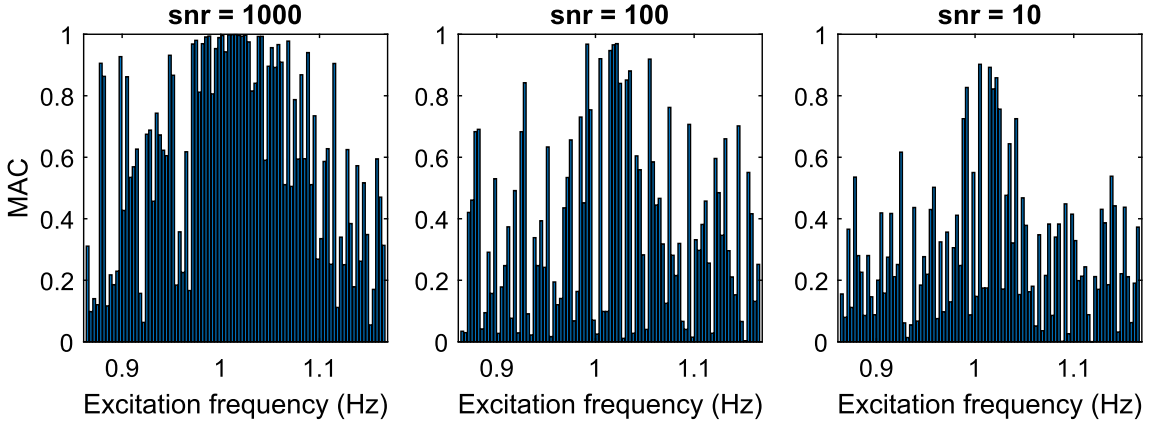

Fig. 5. Variations in the MAC values between $\mathbf{u}(\omega_k)$ and ϕ_1.

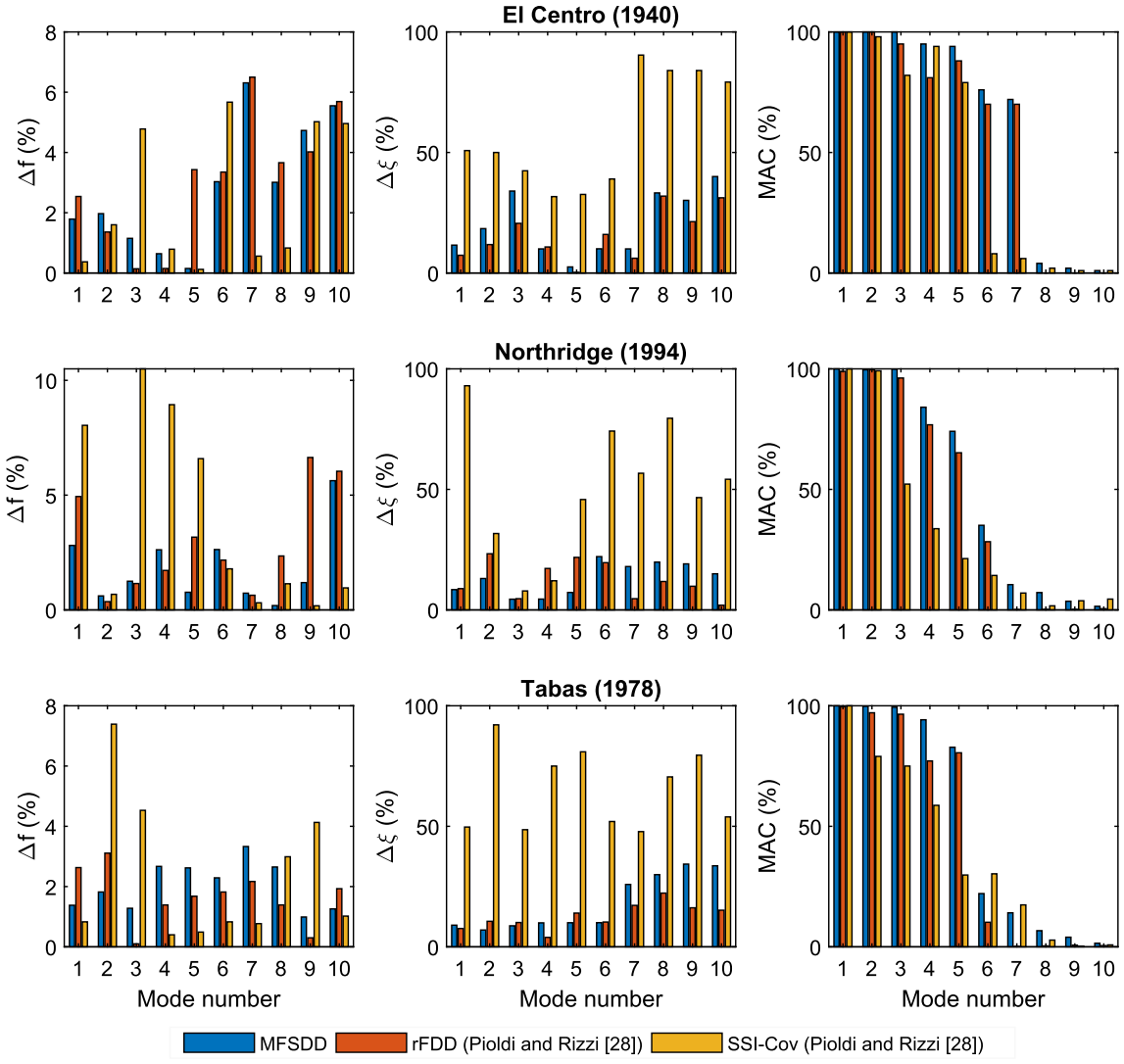

Fig. 6. Variations in the absolute relative errors for the considered earthquakes.

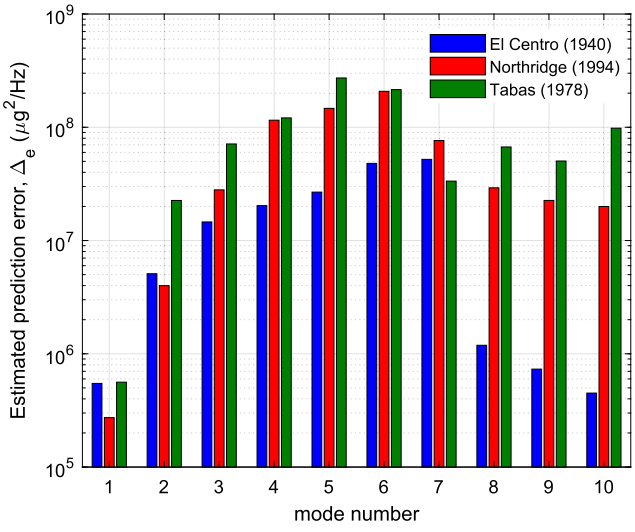

Fig. 7. Variations in prediction errors identified by MFSDD for the considered earthquakes.

SSI-Cov. The absolute relative errors in frequencies and damping ratios obtained by MFSDD follow a similar trend with those by rFDD up to the modes 5–6. Identified MAC values, however, show that MFSDD gives more accurate results than rFDD and SSI-Cov. Here, a dramatical decrease is observed in the quality of identified mode shapes at the higher modes, for all the considered methods.

In MFSDD, the effect of heavy modal damping should be considered as the most important parameter resulting the large modelling errors, since the low damping ratio assumption is highly violated. Specifically, the larger the modal damping, the lower the signal quality, and this ends up with a noisy measurement data. Additionally, the spectral density of modal excitation will tend to show a decrease at higher modes due to the spatial distribution of earthquake loads during the base excitation. This situation may also cause weakly excited modes at higher frequencies, and again a noisy data may appear at the higher modes. On the other hand, when the mode shape orthogonality condition is not satisfied, again large errors might be observed due to the close modes (for the considered example, phase angles between the mode shapes vary in the range of 40-45°).

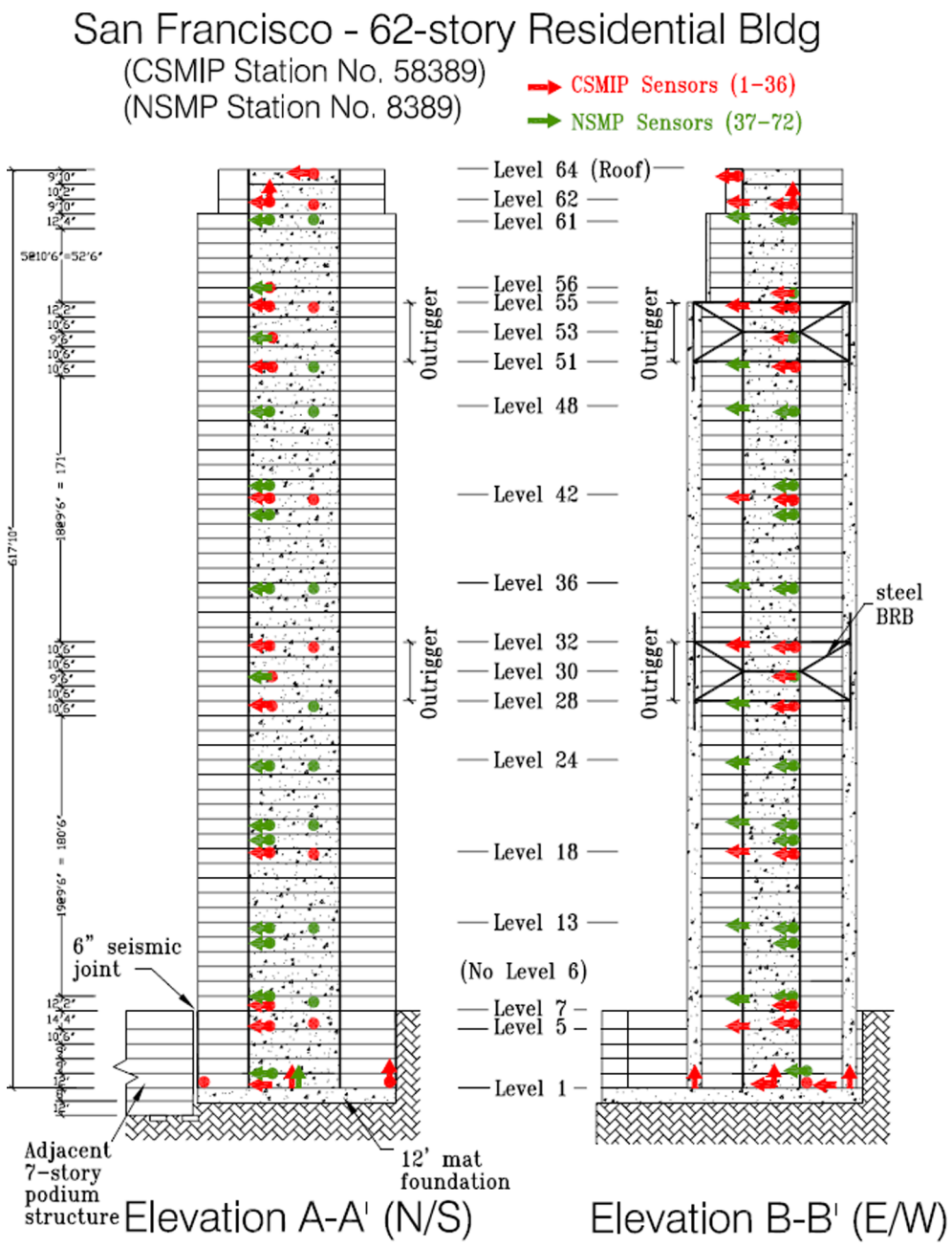

Fig. 8. Elevation view of One Rincon Tower and sensor locations [37].

It should be noted that there is no additional measurement noise (channel noise) defined for the simulated response. From this aspect, it will be more accurate to classify the noisy plots appear in SV spectrum as the effects induced by the modelling errors rather than the measurement noise. In the other words, it can be deduced that the identified prediction errors directly reflect the noise effects induced by the modelling errors for this particular example. In this context, variations in the estimated modelling errors, obtained by MFSDD, are presented in Fig. 7. Here, the identified modelling errors gradually increase till to the modes 5–6. Then, estimated prediction errors follow a more erratic trend due to the significant decrease in the signal quality, as compatible with the results presented in Fig. 6. At higher modes, the accuracy of prediction error is also adversely affected by the large amount of actual modelling errors.

5.3. Experimental analysis 1: One Rincon Tower

In this section, modal properties of a 62-story residential building, One Rincon Tower, are investigated by using MFSDD. The structural system of the investigated building consists of a dual core wall and outriggers. A 72-channel acceleration response monitoring system has been previously installed in the context of a project by the California Strong Motion Instrumentation Program (CSMIP) of the California Geological Survey and the National Strong Motion Project (NSMP) under the Advanced National Seismic Systems managed by the United States Geological Survey (USGS) [36]. The ambient vibration data used in this study has been provided by the Center of Engineering Strong Motion Data (CESMD) [37]. The schematic view of the building and sensor locations are indicated in Fig. 8.

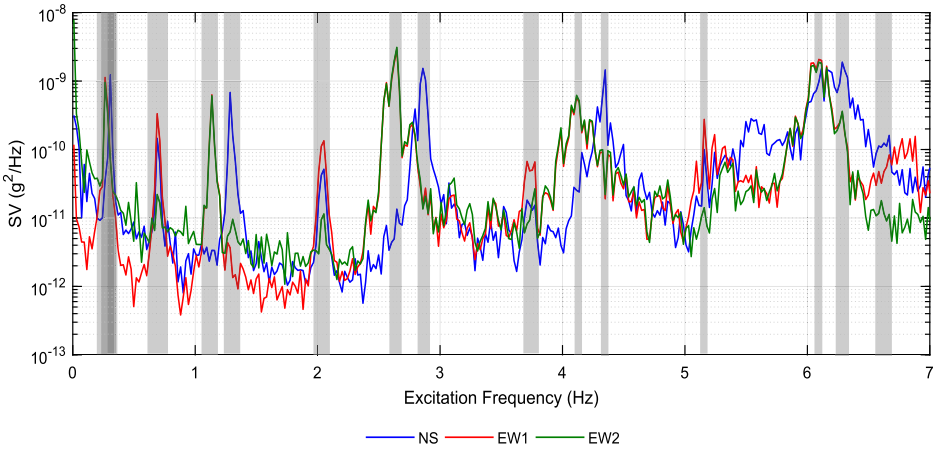

Fig. 9. Maximum singular value spectra obtained for NS, EW1 and EW2 data.

Table 4
Identified modal frequencies and damping ratios for the first fifteen modes.

Mode Number	*f (Hz.)*			*ξ (%)*		
	MFSDD	FSDD	Çelebi et al. [36]	MFSDD	FSDD	Çelebi et al. [36]
1 (EW1-EW2)	0.28–0.28	0.27–0.27	0.27–0.27	1.67–2.39	0.67–0.68	0.90–0.30
2 (NS)	0.31	0.31	0.30	1.07	0.15	0.90
3 (Torsional)	0.71	0.31	0.70	0.76	0.17	0.40
4 (EW1-EW2)	1.14–1.14	1.14–1.14	1.14–1.14	0.55–0.59	0.66–0.49	4.4–2.1
5 (NS)	1.30	1.29	1.30	0.60	0.13	0.50
6 (Torsional)	2.04	0.14	2.04	0.53	0.27	0.48
7 (EW1-EW2)	2.63–2.63	2.64–2.64	2.59–2.59	1.04–1.00	0.20–0.19	0.30–0.30
8 (NS)	2.86	2.87	2.83	0.73	0.53	0.90–1.30
9 (Torsional)	3.74	0.26	3.72	0.86	1.63	1.30
10 (EW1-EW2)	4.12–4.12	4.12–4.12	4.12–4.12	1.09–1.11	1.16–1.17	0.90–0.13
11 (NS)	4.34	4.35	4.34	1.84	1.79	1.70
12 (Torsional)	5.21	0.33	5.17	1.26	2.68	2.60
13 (EW1-EW2)	6.09–6.09	6.06–6.06	6.04–5.39	1.09–1.12	1.36–4.53	5.90–0.70
14 (NS)	6.29	5.93	6.10	0.94	0.84	1.70
15 (Torsional)	6.77	6.81	6.74	1.87	3.09	2.60

Ambient acceleration responses of the investigated structure have been measured in North-South (NS) and East-West (EW) directions by the research team of USGS. For comparison purposes, the results previously reported by Çelebi et al. [36] are considered as reference values. Çelebi et al. [36] performed a modal identification procedure based on two dimensional (2D) data acquired in NS, EW, and torsional directions by using SSI-Cov. Therefore, first, a 2D analysis is performed in this study as being compatible with the procedure implemented by Çelebi et al. [36].

The SV spectra obtained for NS, EW1 and EW2 data are presented in Fig. 9. According to the presented spectra, totally fifteen, well-separated peaks can be detected as possible modes. These possible modes and selected frequency bands are also indicated in the plotted spectrum.

Table 4 presents the modal frequencies and damping ratios identified by MFSDD and FSDD, using 2D data. In general sense, both methods give similar results for the modal frequencies, and match with the results reported by Çelebi et al. [36]. Some major deviations, however, are observed for the identified damping ratios. According to the existing literature, it is well-known that the identifying the modal damping ratios perfectly is a challenging issue in the operational modal analysis [32]. Therefore, the identified modal damping ratios may also show significant variations as depending on the implemented identification technique. In this context, it can be considered that the observed deviations are in a reasonable range for the investigated structure.

The modes shapes estimated by MFSDD and FSDD show a good match with each other, as indicated in Fig. 10. Here, the mode shapes by FSDD are obtained by a trial and error procedure to achieve the best result. For higher modes, this trial–error procedure becomes necessary due the large fluctuations in the quality of mode shapes at the selected discrete excitation frequencies. In addition, the presented mode shapes also match well with the reference results, except for EW1 and EW2. At the second and fifth modes for EW1, and fifth mode for EW2, the results by Çelebi et al. [36] have some distortions, which are not compatible with the mode shapes obtained by MFSDD and FSDD.

A three-dimensional (3D) MFSDD analysis is also performed, considering the all measurement data in the identification process. In comparison to 2D analysis, this procedure is more difficult since some closely spaced modes appear, as seen on the SV spectra presented in Fig. 11. The presented spectra only display the largest three SVs to represent the possible modes in EW, NS and torsional directions. Here, two closely spaced modal peaks are visible around the frequencies of 0.27 and 0.31 Hz, respectively. These modes can also be investigated separately, assigning different and very narrow bandwidths for each one. This selection, however, may not be able to identify the possible mode at 0.30 Hz since it is highly dominated by the mode around the 0.27 Hz. On the other hand, selecting a bandwidth spanning the both peaks, gives very reasonable results by MFSDD as similar with 2D analysis.

Identification results including 3D mode shapes, modal frequencies and damping ratios, are also presented in Fig. 12. Here, it is observed

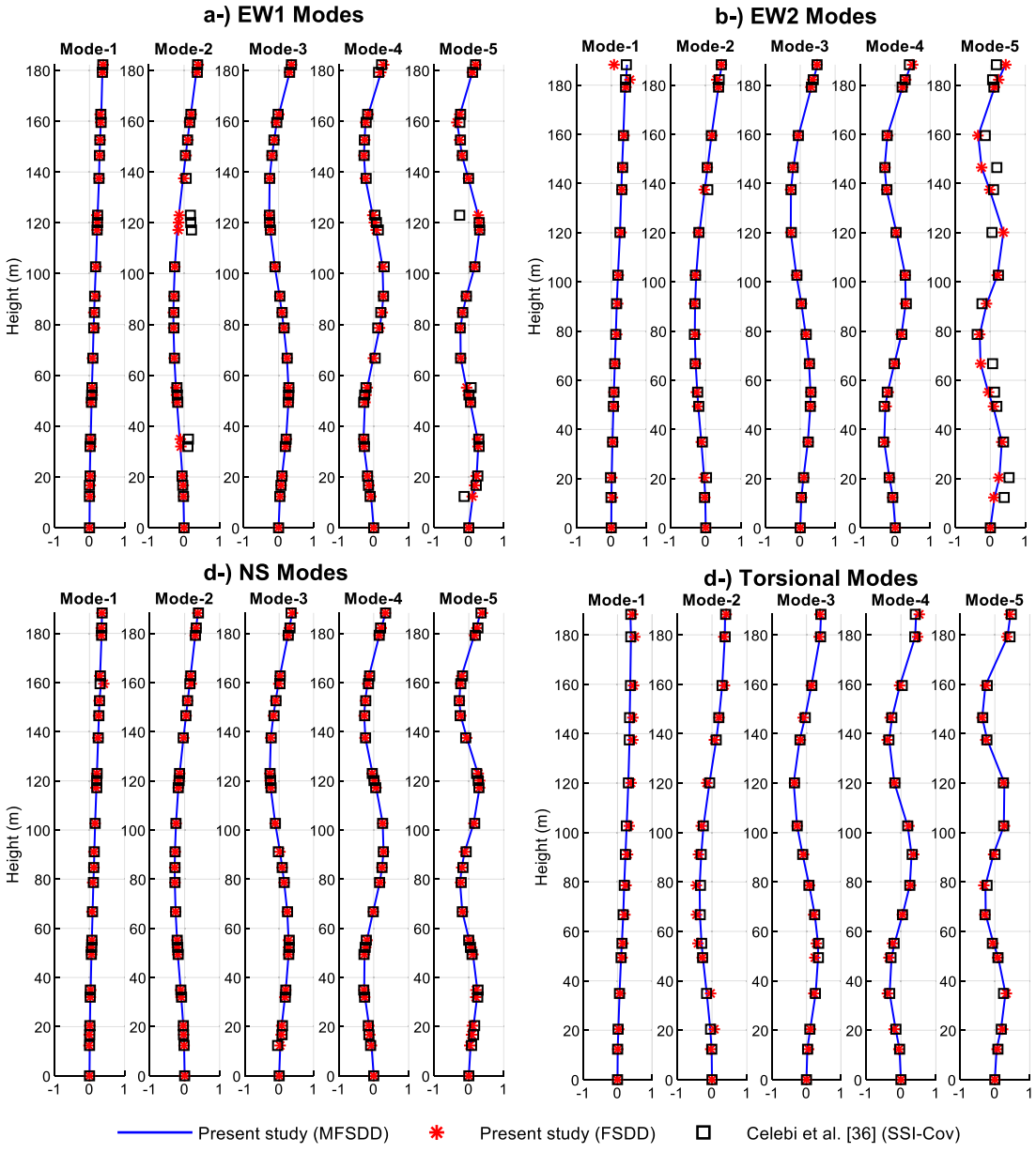

Fig. 10. Identified mode shapes by using EW1, EW2 and NS data.

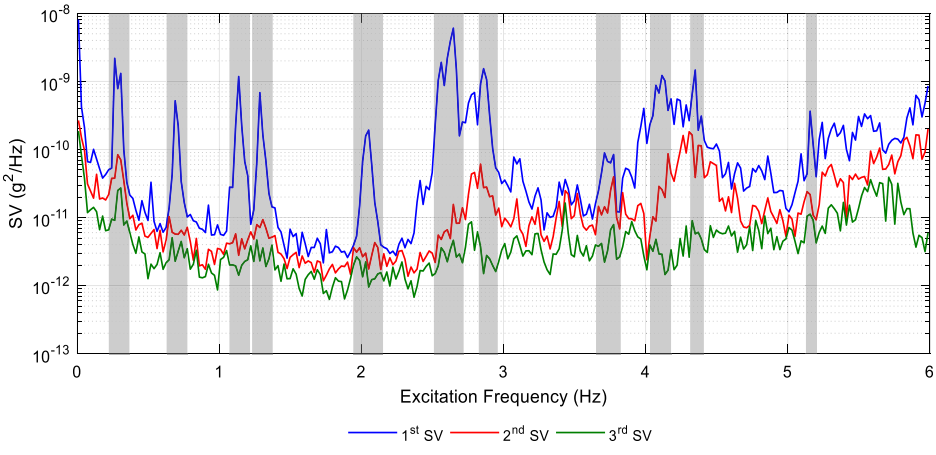

Fig. 11. Singular value spectra and selected bandwidths for 3D analysis.

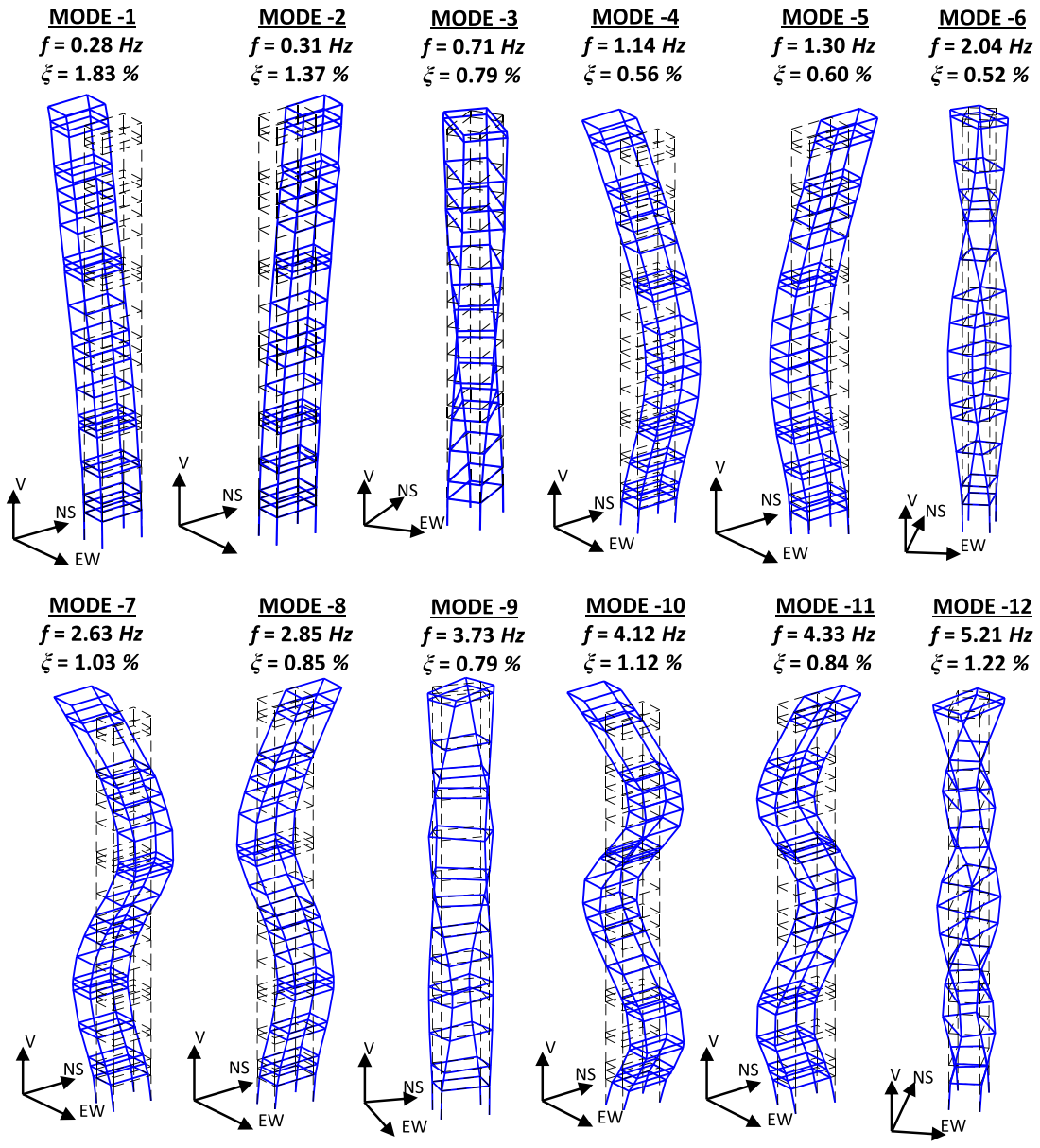

Fig. 12. Identified 3D mode shapes.

that the estimated parameters have a good agreement with 2D analysis results, for all identified modes. Note that the closely spaced modes at 0.27 and 0.30 Hz appear in the perpendicular directions (NS and EW), which results in perfectly orthogonal mode shapes. Thus, it is apparent that MFSDD can make very good estimates for the closely spaced modes when the modelling assumptions are satisfied.

5.4. Experimental analysis 2: Benchmark study

In this section, a modal parameter analysis is performed for a benchmark study which has been widely investigated in the literature. The structure, whose schematic representation is given in Fig. 13, was formerly known as Z24 highway bridge that connects the two towns of Utzenstorf and Koppigen in Switzerland. The bridge has been

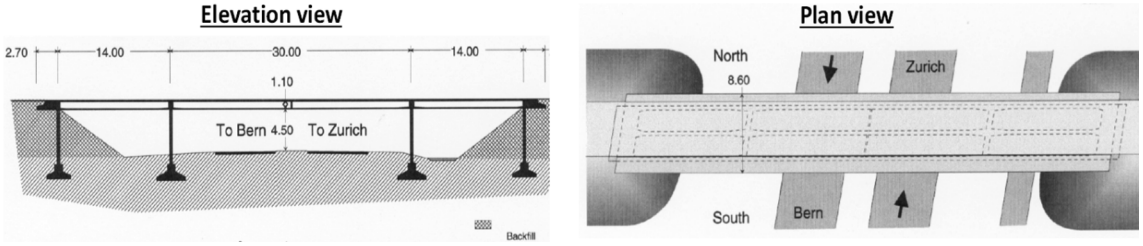

Fig. 13. Schematic representation of Z24 bridge [38].

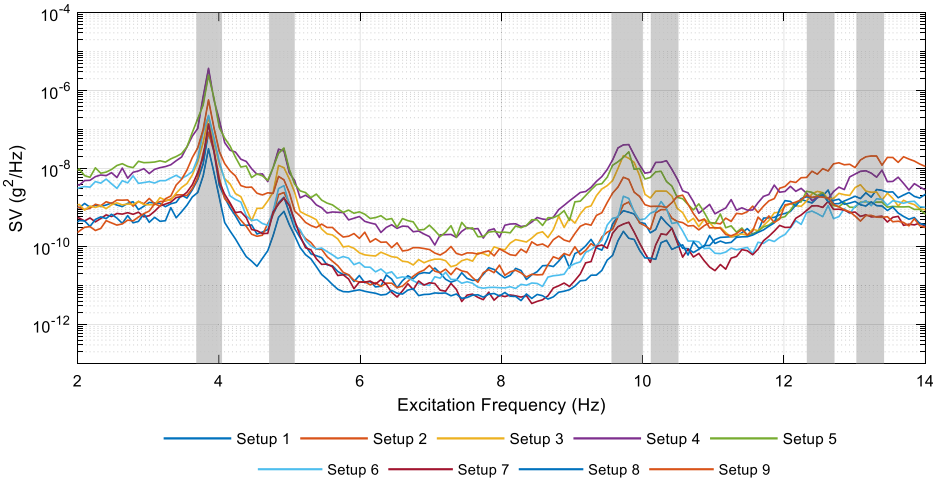

Fig. 14. Singular value spectra and selected bandwidths.

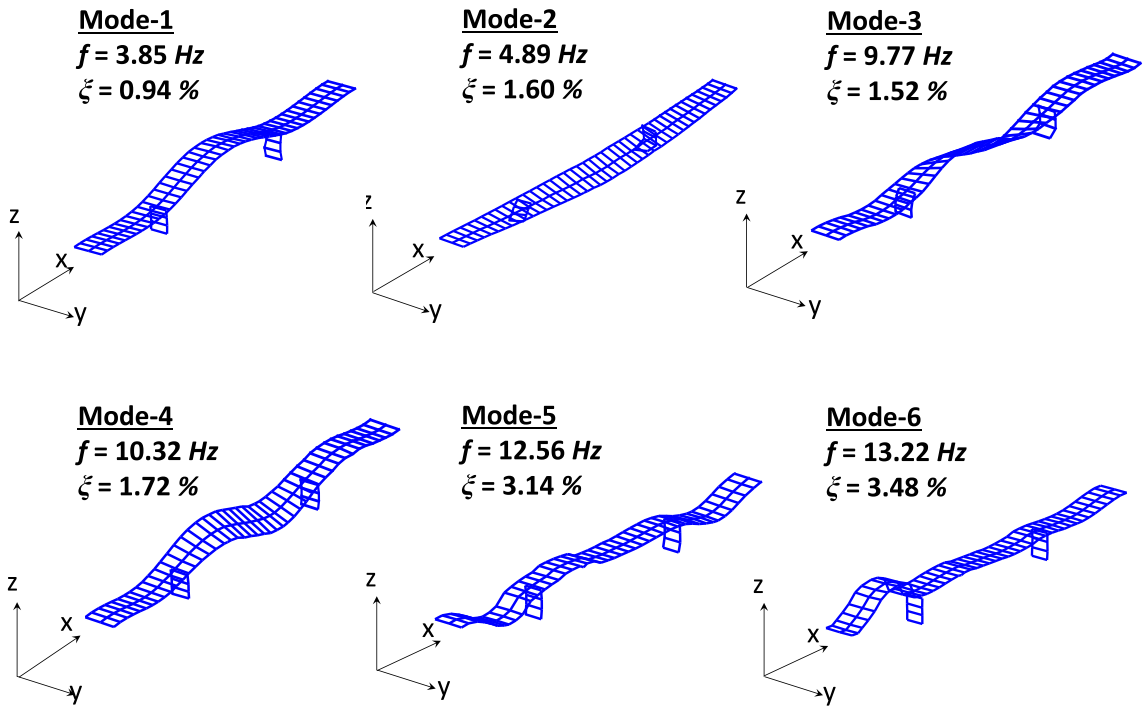

Fig. 15. Identified mode shapes, natural frequencies and modal damping ratios.

demolished after a comprehensive research undertaken by KU LUEVEN Structural Mechanics Division. As a part of their research, the Z24 Bridge was measured by totally nine measurement setups with three constant measurement points. In this study, the second reference measurements are considered among totally eighteen measurement sets, each representing a different damage scenario.

Fig. 14 displays the SV spectra obtained from all setups for the second reference measurements. Possible vibration modes, and selected bandwidths are also indicated in the presented figure. Totally six possible and well-separated modes are visible on the displayed spectra. Considerably large quality of signal levels and easily perceptible modal peaks appear till to the fourth mode. Then, noisy plots are visible, which make it more difficult to identify the possible modes.

In the performed identification procedure, first, the local modal parameters are estimated for each measurement setup. Then, a global value is evaluated for modal frequencies and damping ratios by taking the ensemble average. For the mode shapes, however, this averaging procedure cannot be implemented as each local mode shape corresponds to the different part of the bridge. Instead, global mode shape vectors are estimated by assembly of the local mode shapes using Global Least Squares approach [39].

The assembled mode shapes as well as the estimated natural frequencies, and modal damping ratios are presented in Fig. 15. Modal properties of Z24 bridge was previously investigated by Hızal et al. [14], using Bayesian Mode Shape Assembly (BMSA) technique, based on the second order statistics of the identified local modal parameters. Here, MAC values between the identified mode shapes and the results reported by Hızal et al. [14] are calculated as 0.998, 0.995, 1.000, 0.999, 0.991, 0.993. In addition, Fig. 16 shows a graphical comparison between the identified modal frequencies and damping ratios, and the results reported by [14] and [40]. According to the presented graph, very slight deviations are observed between the estimated and reference modal parameter values.

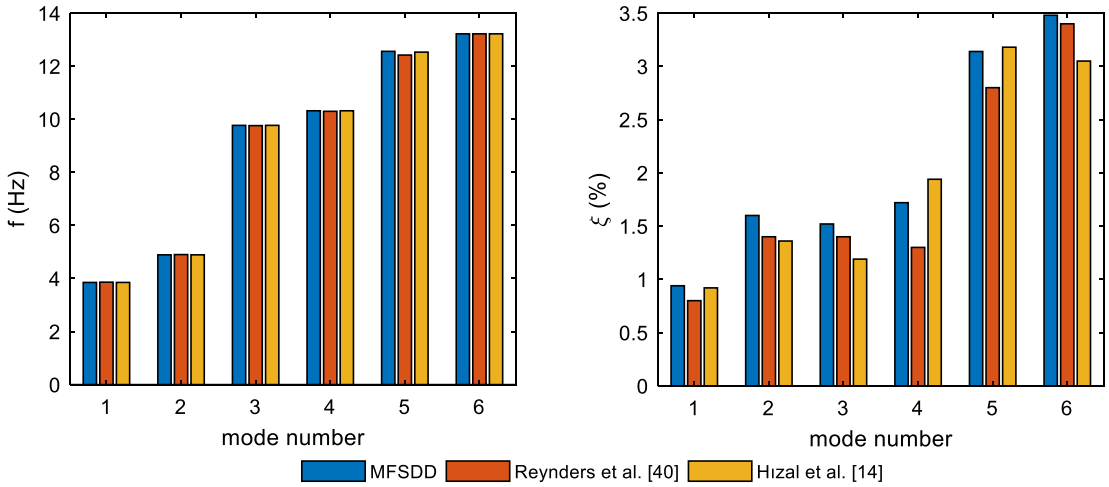

Fig. 16. Comparison of identified natural frequencies and damping ratios.

6. Conclusions

A maximum likelihood matrix estimation based MFSDD technique is presented in this study. Different from the available FDD techniques, a prediction error term is defined in the estimation of output PSD, associating with measurement noise and modelling errors. After the manipulation of proposed maximum likelihood estimator, the optimal modal shape vectors as well as the prediction errors are obtained as closed-form solutions. Then, modal frequencies and damping ratios are updated by minimizing a condensed likelihood function. The presented method is validated by using two numerical and two field data examples. The fundamental results are summarized below.

- Under the large measurement noise effect, the proposed MFSDD technique gives much better results with respect to FSDD, especially for mode shapes. As the measurement noise is not related with modelling assumptions, it produces a biased error in the estimation of output PSD. MFSDD is rather successful to identify those measurement errors provided that the modelling assumptions are satisfied well.
- Identifying the modelling errors becomes much more challenging issue, compared to the measurement noise. Although the identification results by MFSDD show good convergence with actual values for the lower modes in the second numerical example, the estimation quality significantly drops due to the effect of increasing modelling errors at the higher modes. Here, highly damped, closely spaced and weakly excited modes may produce large modelling errors which cannot be identified effectively.
- According to the results obtained from field data examples, it can be concluded that MFSDD can provide reliable estimations for real data applications, including closely spaced modes and/or noisy measurements. Similar to available FDD methods, MFSDD also gives more accurate results when the closely space modes are perfectly orthogonal to each other. In case of these modes are not perfectly orthogonal, the modelling errors may inevitably increase, leading to poor modal estimates.

Declaration of Competing Interest

The author declares that there is no known conflict of interest that can inappropriately influence this work.

References

[1] Caicedo JM. Practical guidelines for the natural excitation technique (NExT) and the eigensystem realization algorithm (ERA) for modal identification using ambient vibration. Exp Tech 2011;35:52–8. https://doi.org/10.1111/j.1747-1567.2010.00643.x.
[2] Van Overschee P, De Moor B. Subspace algorithms for the stochastic identification problem. Automatica. 1993;29:649–60. https://doi.org/10.1016/0005-1098(93)90061-W.
[3] Peeters B, De Roeck G. Reference-Based Stochastic Subspace Identification for Output-Only Modal Analysis. Mech. Syst. Signal Process. 1999;13:855–78. https://doi.org/10.1006/mssp.1999.1249.
[4] Yuen KV, Katafygiotis LS. Bayesian time-domain approach for modal updating using ambient data. Probabilistic Eng. Mech. 2001;16:219–31. https://doi.org/10.1016/S0266-8920(01)00004-2.
[5] Brincker R, Andersen P, Jacobsen NJ. Automated frequency domain decomposition for operational modal analysis. Conf. Proc. Soc. Exp. Mech. Ser. 2007.
[6] Hermans L, Van Der Auweraer H, Guillaume P. A frequency-domain maximum likelihood approach for the extraction of modal parameters from output-only data. Proc. 23rd Int. Conf. Noise Vib. Eng. ISMA. 1998:963–72.
[7] Devriendt C, Guillaume P. Identification of modal parameters from transmissibility measurements. J Sound Vib 2008;314:343–56. https://doi.org/10.1016/j.jsv.2007.12.022.
[8] Devriendt C, Guillaume P. The use of transmissibility measurements in output-only modal analysis. Mech. Syst. Signal Process. 2007;21:2689–96. https://doi.org/10.1016/j.ymssp.2007.02.008.
[9] Yan WJ, Ren WX. An Enhanced Power Spectral Density Transmissibility (EPSDT) approach for operational modal analysis: Theoretical and experimental investigation. Eng Struct 2015;102:108–19. https://doi.org/10.1016/j.engstruct.2015.08.009.
[10] Au S-K. Fast Bayesian FFT Method for Ambient Modal Identification with Separated Modes. J Eng Mech 2011;137:214–26. https://doi.org/10.1061/(asce)em.1943-7889.0000213.
[11] Katafygiotis LS, Yuen KV. Bayesian spectral density approach for modal updating using ambient data. Earthq. Eng. Struct. Dyn. 2001;30:1103–23. https://doi.org/10.1002/eqe.53.
[12] Au SK, Zhang FL. Fast Bayesian Ambient Modal Identification Incorporating Multiple Setups. J Eng Mech 2012;138:800–15. https://doi.org/10.1061/(asce)em.1943-7889.0000385.
[13] Yan WJ, Katafygiotis LS. A two-stage fast Bayesian spectral density approach for ambient modal analysis. Part II: Mode shape assembly and case studies. Mech. Syst. Signal Process. 2015;54:156–71. https://doi.org/10.1016/j.ymssp.2014.08.016.
[14] Hızal Ç, Turan G, Aktaş E, Ceylan H. A mode shape assembly algorithm by using two stage Bayesian Fast Fourier Transform Approach. Mech. Syst. Signal Process. 2019;134:106328. https://doi.org/10.1016/j.ymssp.2019.106328.
[15] Zhang FL, Au SK. Fundamental two-stage formulation for Bayesian system identification, Part II: Application to ambient vibration data. Mech. Syst. Signal Process. 2016;66–67:43–61. https://doi.org/10.1016/j.ymssp.2015.04.024.
[16] Hızal Ç, Turan G. A two-stage Bayesian algorithm for finite element model updating by using ambient response data from multiple measurement setups. J Sound Vib 2020;469:115139. https://doi.org/10.1016/j.jsv.2019.115139.
[17] Gade S, Møller NB, Herlufsen H, Konstantin-Hansen H. Frequency domain techniques for operational modal analysis. Proc. 1st Int Oper. Modal Anal. Conf. IOMAC 2005 2005.
[18] Brincker R, Ventura CE, Andersen P. Damping estimation by frequency domain decomposition. Proc. Int. Modal Anal. Conf. - IMAC. 2001;1:698–703.
[19] Jacobsen NJ, Andersen P, Brincker R. Using enhanced frequency domain decomposition as a robust technique to harmonic excitation in operational modal analysis. Proc. ISMA2006 Int. Conf. Noise Vib. Eng. 2006;6:3129–40.
[20] Brincker R, Zhang L, Andersen P. Modal identification of output-only systems using frequency domain decomposition. Smart Mater Struct 2001;10:441–5. https://doi.org/10.1088/0964-1726/10/3/303.

[21] Zhang L, Wang T, Tamura Y. A frequency-spatial domain decomposition (FSDD) method for operational modal analysis. Mech. Syst. Signal Process. 2010;24:1227–39. https://doi.org/10.1016/j.ymssp.2009.10.024.
[22] L. Zhang, T. Wang, Y. Tamura, A frequency-spatial domain decomposition (FSDD) technique for operational modal analysis, Proc. 1st Int. Oper. Modal Anal. Conf. IOMAC 2005. (2005).
[23] Wang T, Celik O, Catbas FN, Zhang LM. A frequency and spatial domain decomposition method for operational strain modal analysis and its application. Eng Struct 2016;114:104–12. https://doi.org/10.1016/j.engstruct.2016.02.011.
[24] Pioldi F, Ferrari R, Rizzi E. Output-only modal dynamic identification of frames by a refined FDD algorithm at seismic input and high damping. Mech. Syst. Signal Process. 2016;68–69:265–91. https://doi.org/10.1016/j.ymssp.2015.07.004.
[25] Pioldi F, Rizzi E. A refined Frequency Domain Decomposition tool for structural modal monitoring in earthquake engineering. Earthq. Eng. Eng. Vib. 2017;16:627–48. https://doi.org/10.1007/s11803-017-0394-9.
[26] Pioldi F, Ferrari R, Rizzi E. Seismic FDD modal identification and monitoring of building properties from real strong-motion structural response signals. Struct. Control Heal. Monit. 2017;24:1–20. https://doi.org/10.1002/stc.1982.
[27] Pioldi F, Ferrari R, Rizzi E. Earthquake structural modal estimates of multi-storey frames by a refined Frequency Domain Decomposition algorithm. J Vib Control 2017;23:2037–63. https://doi.org/10.1177/1077546315608557.
[28] Pioldi F, Rizzi E. Earthquake-induced structural response output-only identification by two different Operational Modal Analysis techniques. Earthq. Eng. Struct. Dyn. 2018;47:257–64. https://doi.org/10.1002/eqe.2947.
[29] Pioldi F, Rizzi E. Assessment of Frequency versus Time Domain enhanced technique for response-only modal dynamic identification under seismic excitation. Bull Earthq Eng 2018;16:1547–70. https://doi.org/10.1007/s10518-017-0259-7.
[30] Pioldi F, Rizzi E. Full Dynamic Compound Inverse Method for seismic output- only element-level and input identification : Unitary formulation and extensive validation. Mech. Syst. Signal Process. 2018;111:580–614. https://doi.org/10.1016/j.ymssp.2018.04.013.
[31] Yuen K. Bayesian methods for structural dynamics and civil engineering. John Wiley & Sons (Asia) Pte Ltd; 2010.
[32] Au SK. Operational modal analysis: Modeling, bayesian inference, uncertainty laws. Singapore: Springer; 2017. https://doi.org/10.1007/978-981-10-4118-1.
[33] Schott JR, Harville DA. Matrix algebra from a statistician's perspective. Springer; 2006. https://doi.org/10.2307/2669871.
[34] MATLAB 2018a (Computer Software), MathWorks, Natick, MA, (2018).
[35] Villaverde R, Koyama LA. Damped Resonant Appendages to Increase Inherent Damping Buildings. Earthq. Eng. Struct. Dyn. 1993;22:491–507. https://doi.org/10.1002/eqe.4290220603.
[36] Çelebi M, Huang M, Shakal A, Hooper J, Klemencic R. Ambient response of a unique performance-based design tall building with dynamic response modi fi cation features. Struct. Des. Tall Spec. Build. 2013;22:816–29. https://doi.org/10.1002/tal.1093.
[37] United States Geological Survey, Center of Engineering Strong Motion Data, (2020). www.strongmotioncenter.org (accessed September 5, 2018).
[38] Reynders E, De Roeck G. Reference-based combined deterministic – stochastic subspace identification for experimental and operational modal analysis. Mech. Syst. Signal Process. 2008;22:617–37. https://doi.org/10.1016/j.ymssp.2007.09.004.
[39] Au SK. Assembling mode shapes by least squares. Mech. Syst. Signal Process. 2011;25:163–79. https://doi.org/10.1016/j.ymssp.2010.08.002.
[40] Reynders E, Houbrechts J, De Roeck G. Fully automated (operational) modal analysis. Mech. Syst. Signal Process. 2012;29:228–50. https://doi.org/10.1016/j.ymssp.2012.01.007.